How do the electronic properties of d^9 impurities depend on metal-ligand distances? Application to Ni$^+$, Cu^{2+} and Ag^{2+} systems

How do the electronic properties of d⁹ impurities depend on metal–ligand distances? Application to Ni⁺, Cu²⁺ and Ag²⁺ systems

J A Aramburu†, M Moreno† and M T Barriuso‡

† DCITTYM, Sección Ciencia de Materiales, Facultad de Ciencias, Universidad de Cantabria, 39005 Santander, Spain
‡ Departamento de Física Moderna, Facultad de Ciencias, Universidad de Cantabria, 39005 Santander, Spain

Abstract. The dependence of the optical and spin-Hamiltonian parameters of NiF_6^{5-} and NiF_4^{3-} D_{4h} units, with a b_{1g}^* ($\sim x^2 - y^2$) unpaired electron, upon the equatorial (R_{eq}) and axial (R_{ax}) Ni⁺–F⁻ distances has been studied through multiple-scattering $X\alpha$ and self-consistent charge extended Hückel methods. *Both* methods lead to the following main conclusions: (i) A charge-transfer transition like $e_u(\pi + \sigma, \text{eq}) \rightarrow b_{1g}^*$ ($\sim x^2 - y^2$) (termed E_u) is more sensitive than a crystal-field one like b_{2g}^* ($\sim xy$) $\rightarrow b_{1g}^*(\Delta_1)$ or $e_g^* \rightarrow b_{1g}^*(\Delta_2)$ to variations in R_{eq}. The change experienced by E_u mainly reflects that of $V_{el}(M) - V_{el}(L)$, where $V_{el}(M)$ and $V_{el}(L)$ are the electrostatic potentials experienced by an electron placed on metal and ligands, respectively. (ii) As regards the unpaired spin densities onto n_Lp and n_Ls ligand valence orbitals (termed f_σ and f_s respectively), it is found that $f_\sigma \gg f_s$ but f_s is much more sensitive to changes in R_{eq}. The microscopic origin of this relevant fact is explained in detail. (iii) The removal of axial ligands, keeping R_{eq} constant, induces a decrease of E_u as a result of the diminution of the electrostatic repulsion, $V_{el}(M)$, and produces a slight increase of Δ_1 and a more important one of Δ_2. (iv) The dependence of $g_\parallel - g_0$ and $g_\perp - g_0$ on R_{eq} essentially reflects that of Δ_1^{-1} and Δ_2^{-1}, respectively, because of the low covalency ($f_\sigma \simeq 2\%$).

These results on NiF_6^{5-} and NiF_4^{3-} explain the main differences displayed by the electron paramagnetic resonance parameters of Ni⁺(I) and Ni⁺(III) centres in fluoroperovskites, respectively, only on the basis of the host lattice dependence of R_{eq}. Furthermore, they support the determination of the true R_{eq} through the experimental isotropic superhyperfine constant, A_s. The experimental g-tensor values of Ni⁺ centres are well understood through our calculations, which involve no adjustable parameters at all, and demonstrate that (i) Ni⁺(III) and Ni⁺(I) centres can be distinguished by looking only at the experimental $g_\perp$ value, (ii) aside from inducing a decrement of R_{eq}, the main effects due to axial vacancies are the diminution of the electrostatic repulsion $V_{el}(M)$ as well as the breaking of bonds with axial ligands in the e_g^* orbital, and (iii) changes of R_{eq} of 0.1 pm can be detected through $g_\parallel$ provided an uncertainty of $\pm 10^{-3}$ is reached. The trends derived from this study are shown to be followed also by Cu²⁺ and Ag²⁺ systems, with moderate covalency. In particular, it is now reasonably explained why CdCl₂:Cu²⁺ and (N-mpH)₂CuCl₄ have the same E_u value while Δ_1 and Δ_2 are clearly higher for the latter system.

1. Introduction

A *basic* understanding of the properties of a doped crystalline material is, in principle, more difficult than for a pure one because of the lack of periodicity. In the case of

impurities in insulators and ionic semiconductors, this general situation is, however, greatly simplified. In fact, the electronic properties due, for instance, to a transition-metal (TM) impurity, M, can be understood to a great extent *only* on the basis of the ML_n complex formed with the n nearest anions, L. This idea was pointed out by Sugano and Shulman [1] and supported by subsequent work [2–12]. It provides a bridge between the realm of impurities in insulators and that of TM complexes in inorganic chemistry. Despite this relatively simple theoretical framework, the number of attempts devoted to exploring the dependence of a *large number* of optical and electron paramagnetic resonance (EPR) parameters corresponding to a d impurity on the M–L distance, R, has been up to now, rather limited. This task is compulsory, however, for gaining a good insight into the variations undergone by spectroscopic *parameters under applied pressures or temperature changes*. Furthermore, it can help us to solve one of the fundamental problems in the domain of impurities: to determine what is the *true* R value and the *true* variations, ΔR, experienced by the M–L distance upon pressure or temperature changes. The importance of investigation in this realm has been demonstrated, for instance, in the case of Mn^{2+}-doped fluorides, where true R values have been derived from the experimental isotropic superhyperfine (SHF) constant [13], A_s, and the cubic field splitting [14, 15], $10Dq$, while the anisotropic SHF constant, A_{an}, has been shown [7] to be less sensitive to changes in R. Furthermore, in such systems, whose present situation is reviewed in [16], ΔR values down to ~ 0.1 pm can be well detected by monitoring the corresponding variations of A_s and $10Dq$, thus *improving* by an order of magnitude the limit reached through extended x-ray absorption fine structure (EXAFS), which is about 2 pm. Therefore, in the case of TM impurities, the variations ΔR induced by applied pressures smaller than ~ 5 GPa, structural phase transitions of the host lattice or normal thermal expansion effects cannot be detected by means of EXAFS whereas they can indeed be observed using optical and EPR parameters.

This work is devoted to exploring the dependence of optical and EPR parameters of d^9 impurities on impurity–ligand distances. Although d^9 ions involve one unpaired electron and thus exhibit a relatively simple electronic structure, it is difficult to observe them in a cubic environment because of the Jahn–Teller theorem [17]. Owing to this fact, the final local geometry reached by a d^9 ion placed in an 'initial' pure octahedral site corresponds very often to an elongated octahedral situation with four closer equatorial ligands at R_{eq} and two further axial ligands situated at R_{ax}. Therefore, a good insight into the properties of d^9 ions in insulators requires analysis of how they depend on *both* the equatorial (R_{eq}) and axial (R_{ax}) metal–ligand distances, and it is one of the main goals of the present work.

To accomplish this task we have first addressed our attention to Ni^+ centres in fluoroperovskites [18–21]. In the case of $KMgF_3$, K_2MgF_4 and $RbCaF_3$ lattices, *three* kinds of *simple* Ni^+ centres (figure 1) have been *well identified* [12–14] through the experimental SHF and g-tensors measured by EPR. Centre I can be described as a NiF_6^{5-} complex displaying an elongated octahedral geometry as a direct consequence of the Jahn–Teller effect and random strains. Centres II and III involve the presence of one and two axial vacancies, respectively.

We have also investigated the Ni^+ centres found in CaF_2 [22] and SrF_2 [23] whose local geometry is very close to that of a NiF_4^{3-} square-planar complex characterizing centre III in fluoroperovskites. A similar geometry was encountered for Cu^{2+} [24] and Ag^{2+} [25, 26]. Although this geometry gives rise to a singlet orbital ground state, it cannot be properly said that $CaF_2:Ni^{2+}$, $SrCl_2:Ag^{2+}$, etc, are the result of
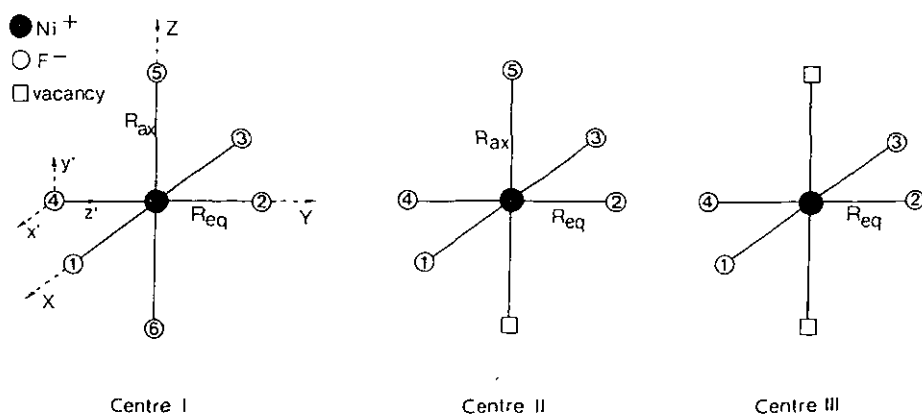
Figure 1. Structure of the three Ni$^+$ centres discovered in fluoroperovskites. The unpaired electron is always placed in a $x^2 - y^2$ type orbital.

the Jahn–Teller effect, as this effect is mentioned when displacements from the initial cubic position are small while in the latter cases the cation undergoes displacements higher than 1 Å.

To analyse whether the rich experimental information on Ni$^+$ in fluorides can be understood mainly on the basis of different R_{eq} and R_{ax} distances for all Ni$^+$ systems is the main purpose of the present work. If the electrostatic potential exerted by the rest of the lattice is not constant in the complex, differences corresponding to a ML$_n$ complex embedded in two different lattices cannot be explained only in terms of *isolated* ML$_n$ units with different M–L distances. This effect plays an important role in explaining the differences shown by optical spectra of K$_2$NaCrF$_6$ and CrF$_3$ [27]. For the Ni$^+$ centres studied in this work, the host matrix has, however, the same structure, and the potential due to the rest of the lattice is very flat [1]. The existence of extensive experimental information (not existing up to now for Cu^{2+} in fluoroperovskites) together with an early work [28, 29] relating the equatorial A_s value and R_{eq}, explains our initial attention to the unusual Ni$^+$ ion. Nevertheless, the interest of the present study goes beyond the Ni$^+$ centres themselves. In fact, the *main trends* derived from the analysis of Ni$^+$ centres could also serve as a *guide* for understanding the variations of optical and EPR parameters due to other d^9 impurities in different lattices. An application of this idea to Cu^{2+} in several chloride lattices is given in section 6.

In trying to explain the experimental results on Ni$^+$ centres in fluorides, we have, first, carried out self-consistent charge extended Hückel (SCCEH) and multiple-scattering $X\alpha$ (MS-$X\alpha$) calculations for different R_{eq} and R_{ax} values and analysed the dependence of one-electron energies and molecular-orbital (MO) coefficients on both distances. From them, we have derived the dependence of optical transitions as well as that of the [g] and SHF tensors on R_{eq} and R_{ax}. As all the MO methods applied to 3d systems involve approximations, the use of two different methods for the same problem helps significantly to clarify what are the right trends displayed by the dependence of different EPR and optical parameters upon R_{eq} and R_{ax}. The usefulness of this idea was previously shown [30]. Besides the use of two MO methods and the study made on *several* spectroscopic parameters, there is another

characteristic of the present work to be underlined. In fact, a special effort is devoted here to understand what are the *main causes responsible* for the variations of different parameters with R_{eq} and R_{ax}. To accomplish this task, each one-electron energy is expressed as a sum of three contributions whose meaning is detailed in section 4.

2. Experimental information of Ni^+ centres

The action of x-rays on insulator materials doped with Ni^{2+} can give rise to the formation of the 'unstable' Ni^+ cation. The presence of this impurity has usually been confirmed [18–23, 31] through EPR as, up to now, optical data on Ni^+ centres are scarce. In particular, no optical data on crystal-field transitions are reported up to now. As the Ni nucleus has no magnetic moment, the spin Hamiltonian, H_s, corresponding to Ni^+ centres in fluoroperovskites is simply written as

$$H_s = \beta H [g] S + \sum_k I_k [T_k] S \tag{2.1}$$

where $[T_k]$ describes the SHF interaction with the k-ligand nucleus. For the centres of figure 1 one of the principal directions of the $[T_k]$ tensor is just given by the vector R_k joining the d^9 ion and the k-ligand. Though not required by the symmetry of centres, the experimental diagonalized $[T_k]$ tensor is found to be practically axial, involving the two quantities $A_\parallel$ and $A_\perp$. In the case of $Ni^+(I)$ and $Ni^+(II)$ centres the SHF interaction with equatorial ligands is much stronger [18–20] than that with axial ligands, stressing the planar character of the unpaired electron described by a $x^2 - y^2$ type orbital. Through the present work we shall only be concerned with the SHF tensor of equatorial ligands of all analysed Ni^+ centres. The experimental $[g]$ and SHF tensors for Ni^+ centres in fluoroperovskites are given in table 1, while those corresponding to the nearly square-planar NiF_4^{3-} units formed in CaF_2 and SrF_2 are given in table 2. In both tables are also included the isotropic (A_s) and anisotropic (A_{an}) *first-order* contributions to the SHF tensor, and so $A_\parallel$ and $A_\perp$ can be written as

$$A_\parallel = A_s + 2A_{an} + \delta(A_\parallel)$$
$$A_\perp = A_s - A_{an} + \delta(A_\perp). \tag{2.2}$$

The microscopic expressions of A_s and A_{an} are discussed in section 3 while those for $\delta(A_\parallel)$ and $\delta(A_\perp)$ can be found in the microscopic analysis of spin-Hamiltonian parameters of d^9 systems reported in [32]. In the present cases [33] $\delta(A_\parallel)/A_\parallel$ is about 2% while $\delta(A_\perp)/A_\perp$ is about 12%, and thus such 'corrections' play a non-negligible role in the analysis of the SHF tensor.

Tables 1 and 2 reveal that, for a given type of centre, both $g_\parallel$ and A_s experience significant variations when the host lattice is changed, while A_{an} is clearly much less sensitive. Also an increase of both A_s and A_{an} as well as a decrease of both $g_\parallel$ and $g_\perp$ is reflected in table 1 on passing from centre I to centre III, keeping the same host lattice. The calculations shown in this work look to explain the microscopic origin of these variations.

Table 1. Experimental data of g and SHF tensors for Ni$^+$ centres in fluoroperovskites. The SHF tensor refers only to equatorial ligands and is given in 10^{-4} cm^{-1} units. R_{eq} is the equatorial Ni$^+$–F$^-$ distance calculated in section 5.3, from the experimental A_s values. R_0 corresponds to the metal–ligand distance in the perfect lattice. R_{eq} and R_0 values are given in pm. Errors are given in parentheses.

Host	Centre	$g_\parallel$	$g_\perp$	$A_\parallel$	$A_\perp$	A_{sn}	A_s	R_{eq}	R_0	Ref.
K$_2$MgF$_4$	I	2.614(3)	2.115(3)	8.38(17)	42.8(17)	11.7(11)	59.2(17)	210.1(9)	197.0	19
KMgF$_3$	I	2.657(2)	2.137(2)	74.2(17)	37.1(13)	10.4(10)	52.2(15)	213.9(9)	199.3	18
RbCaF$_3$	I	2.778(3)	2.131(3)	67.8(17)	29.4(17)	10.8(11)	44.9(17)	218.4(12)	222.3	20
K$_2$MgF$_4$	II	2.538(3)	2.116(3)	96.2(17)	41.4(17)	16.3(11)	62.4(17)	208.5(8)	197.0	19
KMgF$_3$	II	2.578(2)	2.106(2)	88.2(13)	39.7(13)	14.2(9)	58.6(13)	210.6(9)	199.3	18
RbCaF$_3$	II	2.688	2.115	73.8(17)	30.1(17)	12.6(11)	47.4(17)	216.8(11)	222.3	20
K$_2$MgF$_4$	III	2.508(5)	2.086(5)	96.5(17)	46.8(17)	14.6(11)	66.1(17)	206.7(8)	197.0	19
KMgF$_3$	III	2.545(5)	2.085(5)	93.5(17)	43.1(13)	14.8(10)	62.6(15)	208.4(9)	199.3	18
RbCaF$_3$	III	2.663	2.114	77.8(17)	31.2(17)	13.6(11)	49.5(17)	215.4(11)	222.3	20
KZnF$_3$	—	2.575(1)	2.088(1)	84.0(20)	46.0(20)	10.7(13)	61.4(20)	208.9(10)	202.8	21

Table 2. Experimental data of g and SHF tensors for Ni^+ centres in fluorite-type lattices, where Ni^+ is surrounded by four F^- ions. The SHF tensor is given in 10^{-4} cm^{-1} units. The meaning of R_{eq} is the same as in table 1. R_0 corresponds to the Ni^+–F^- distance in the perfect lattice assuming that Ni^+ lies at the centre of the square formed by the four F^- ions. R_{eq} and R_0 are given in pm. Errors are given in parenthesis.

Host	$g_\parallel$	$g_\perp$	$A_\parallel$	$A_\perp$	A_s	R_{eq}	R_0	Ref.
CaF$_2$	2.569(5)	2.089(5)	81.3(30)	36.5(30)	54.3(30)	210.9(17)	193.1	22
SrF$_2$	2.597(5)	2.090(5)	78.5(17)	35.1(17)	52.3(17)	212.0(10)	205.0	23

3. Theoretical framework

3.1. One-electron levels of NiF_6^{5-} and NiF_4^{3-} complexes

The one-electron level scheme for an elongated ML_6 complex (M = d^9 ion) neglecting, in a first approximation, the spin–orbit interaction is shown in figure 2. The unpaired electron is placed in the antibonding b_{1g}^* ($\sim x^2 - y^2$) level. Levels like a_{1g}(ax) or a_{1g}(eq) in figure 2 mean that they are mainly built from $n_L p$ valence levels of axial or equatorial ligands, respectively. The situation for a square-planar ML_4 complex is rather similar to that of figure 2 but excluding levels like e_g(ax), a_{2u}(ax), etc.
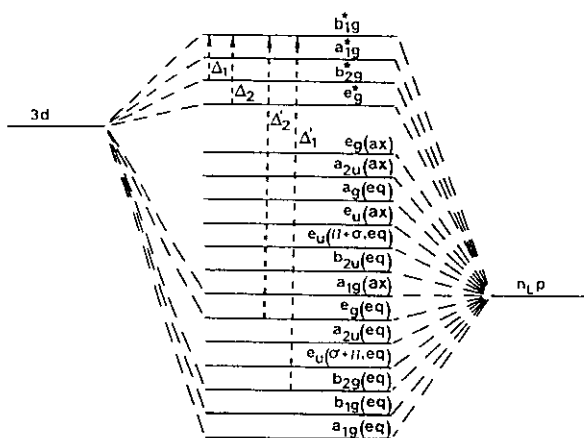

Figure 2. The MO scheme for an elongated ML_6 complex (M = d^9 ion) with D$_{4h}$ symmetry. For simplicity only the d levels of the central ion and the $n_L p$ levels of ligands are included. The ordering of one-electron levels is that obtained from present calculations for NiF_6^{5-}.

Within the framework of MO theory [34] the normalized wavefunction $|b_{1g}^*\rangle$ describing the unpaired electron can be written as

$$|b_{1g}^*\rangle = \alpha_0|d(x^2 - y^2)\rangle - \beta_0(\mu_p|\chi_{p\sigma}\rangle + \mu_s|\chi_s\rangle)$$

$$\mu_p^2 + \mu_s^2 = 1 \tag{3.1}$$

where $|\chi_{p\sigma}\rangle$ and $|\chi_s\rangle$ are linear combinations of $n_L p$ and $n_L s$ equatorial ligand orbitals, respectively, transforming as the B$_{1g}$ representation of D$_{4h}$. Here $S_{p\sigma} =$

$\langle \mathrm{d}(x^2 - y^2)|\chi_{\mathrm{p}\sigma}\rangle$ and $S_{\mathrm{s}} = \langle \mathrm{d}(x^2 - y^2)|\chi_{\mathrm{s}}\rangle$ denote group overlap integrals [34] widely employed throughout the present discussions.

The expressions of $|\chi_{\mathrm{p}\sigma}\rangle$ and $|\chi_{\mathrm{s}}\rangle$, according to the coordinate system of figure 1 and neglecting the ligand–ligand overlap, are

$$|\chi_{\mathrm{p}\sigma}\rangle = (\tfrac{1}{2})[-|\mathrm{p}_x(1)\rangle + |\mathrm{p}_y(2)\rangle + |\mathrm{p}_x(3)\rangle - |\mathrm{p}_y(4)\rangle]$$

$$|\chi_{\mathrm{s}}\rangle = (\tfrac{1}{2})[|\mathrm{s}(1)\rangle - |\mathrm{s}(2)\rangle + |\mathrm{s}(3)\rangle - |\mathrm{s}(4)\rangle].$$

(3.2)

Thus the *same* MO corresponds to the unpaired electron of $\mathrm{NiF_4^{3-}}$ and of the elongated $\mathrm{NiF_6^{5-}}$ complex involving *only* $n_{\mathrm{L}}\mathrm{p}$ and $n_{\mathrm{L}}\mathrm{s}$ levels of equatorial ligands. In the case of crystal-field levels $\mathrm{b_{2g}^*}$ and $\mathrm{e_g^*}$, an expression similar to (3.1) holds but excluding the admixture with $n_{\mathrm{L}}\mathrm{s}$ levels of equatorial ligands. The MO coefficients corresponding to $|\mathrm{b_{2g}^*}\rangle$ and $|\mathrm{e_g^*}\rangle$ are denoted as (α_1, β_1) and (α_2, β_2), respectively. In the case of $\mathrm{NiF_6^{5-}}$ (but not for $\mathrm{NiF_4^{3-}}$) axial ligand orbitals (like $|\mathrm{p}_x(5)\rangle$ and $|\mathrm{p}_x(6)\rangle$) are *also* involved in $|\mathrm{e_g^*}\rangle$, although calculations indicate that in a smaller amount than the equatorial ligand orbitals.

From equations (3.1) and (3.2) the unpaired spin densities, f_σ and f_{s}, on equatorial $n_{\mathrm{L}}\mathrm{p}$ and $n_{\mathrm{L}}\mathrm{s}$ ligand orbitals, are just given by

$$f_\sigma = (\beta_0 \mu_{\mathrm{p}})^2 / 4 \qquad f_{\mathrm{s}} = (\beta_0 \mu_{\mathrm{s}})^2 / 4.$$

(3.3)

When halides are present as ligands, $f_\sigma \gg f_{\mathrm{s}}$ because of the significant difference between the energy of $n_{\mathrm{L}}\mathrm{p}$ and $n_{\mathrm{L}}\mathrm{s}$ levels. For $\mathrm{F^-}$ such a difference amounts to 25 eV.

3.2. Molecular-orbital methods

Calculations of one-electron energies and MO coefficients have been carried out for the *isolated* $\mathrm{NiF_6^{5-}}$ and $\mathrm{NiF_4^{3-}}$ complexes as well as for bigger clusters simulating such complexes inserted in the simple LiF lattice. As explained in a previous work [30], this has been done to verify that $\mathrm{NiF_6^{5-}}$ and $\mathrm{NiF_4^{3-}}$ complexes alone already reproduce the main trends displayed by the spin-Hamiltonian parameters.

To be more sure of the predicted trends, two different MO methods have been used simultaneously: the MS-$X\alpha$ and the SCCEH methods. The biggest cluster studied through the SCCEH method is $\mathrm{NiLi_{42}F_{38}^{5-}}$ while the maximum size cluster calculated through the MS-$X\alpha$ method corresponds to $\mathrm{NiLi_{12}F_{14}^-}$. Although calculated properties like d $\rightarrow$ d and charge-transfer transitions, g-tensor, etc, show the same trends for all studied clusters, they exhibit, however, a slight oscillatory dependence on cluster size, as already found, for instance, by Messmer and Watkins [35]. Besides the analysis of their results being easy, the SCCEH method has the advantage of taking the diagonal elements, h_{ii}, associated with the one-electron Hamiltonian, h, directly from experimental atomic data. Thus problems found in Hartree–Fock–Roothaan calculations of TM complexes derived from the neglect of electronic correlation and the use of simple wavefunctions [11] for describing negative ions (like $\mathrm{F^-}$, $\mathrm{Cl^-}$, etc.) are greatly suppressed in this semiempirical procedure, at least at the atomic level. The expression for h_{ii} is

$$h_{ii} = -\mathrm{VSIE}(q) + V_{\mathrm{el}} + V_{\mathrm{W}}.$$

(3.4)

Here $\text{VSIE}(q)$ (valence state ionization energy [36]) depends on the type of orbital and on the total charge q, of the atom and comes from atomic data. V_{el} denotes the electrostatic interaction between an electron in an atomic orbital i and the non-zero charges of other atoms in the cluster. Finally, V_W corresponds to the electrostatic interaction between the electrons in the cluster and ions lying outside. The off-diagonal matrix elements, h_{ij}, have been calculated using the expression from Ammeter *et al* [37]. Accurate Clementi–Roetti [38] wavefunctions have been used for computing all the overlap integrals of complexes. We have verified that the use of poorer-quality wavefunctions significantly affects the dependence of the spectroscopic parameters upon R_{ax} and R_{eq}. In spite of its simplicity, recent works [39–41] have pointed out the usefulness of the SCCEH method for exploring the main features of insulating systems.

The standard version of the self-consistent field (SCF) MS-$X\alpha$ method [42] was used to carry out spin-restricted calculations on a cluster centred around the nickel. Neutral atoms have been used in the initial atomic calculations to construct the starting molecular potential. The sphere radii of the muffin-tin approximation were determined following completely the Norman procedure [43]: (i) the ratio of the sphere radii was fixed to the ratio of the atomic number radii; (ii) we allow the atomic spheres to overlap; and (iii) the absolute values of the radii have been determined by imposing a virial ratio $-2\langle T\rangle/\langle V\rangle$ to be exactly one. The outer sphere was tangential to the more external fluoride spheres, and the charge of the cluster was stabilized using a Watson sphere of opposite charge with the same radius as the outer sphere.

3.3. The spin-Hamiltonian parameters

The relation between the macroscopic spin-Hamiltonian parameters and microscopic quantities like f_σ, f_s, Δ_1, etc., has been fully discussed in [30, 32] and thus here only the main results will be summarized.

Microscopically the isotropic SHF constant, A_s, corresponding to equatorial ligands reflects, in the present case, the unpaired density spin, f_s, transferred to n_Ls ligand orbitals through the chemical bond [28, 30]. It is simply given by

$$A_s = f_s A_s^0 \tag{3.5}$$

where $A_s^0 = 15\,193 \times 10^{-4}$ cm^{-1} corresponds to the free F$^-$ ion. A similar situation is encountered for TM complexes with octahedral geometry and having unpaired electrons with E$_g$ symmetry [16]. For the present case A_{an} is essentially given [30] by

$$A_{an} = A_\sigma + A_d \tag{3.6}$$

where

$$A_\sigma = f_\sigma A_p^0 \tag{3.7}$$

arises from bonding ($A_p^0 = 463 \times 10^{-4}$ cm^{-1} for the free F$^-$ ion) while

$$A_d = (2\beta\beta_N g_N)\alpha_0^2/R_{eq}^3 \tag{3.8}$$

reflects the magnetic dipolar interaction between the electronic spin on Ni$^+$ and the nuclear spin of a ligand. For the present cases A_{an} is dominated by A_σ. Full

expressions for A_{an} as well as for $\delta A_\parallel$ and $\delta A_\perp$ in equation (2.2) can be found in [32]. Such complete expressions have been used throughout this work for deriving A_s and A_{an} from the experimental $A_\parallel$ and $A_\perp$ values.

As is well known spin–orbit coupling determines the $[g]$ tensor of TM complexes. Up to second order of perturbations only the virtual excitations $b_{2g}^* \to b_{1g}^*$ (termed Δ_1) and $b_{2g}(eq) \to b_{1g}^*$ (termed Δ_1'), in the scheme of figure 2, determine $g_\parallel - g_0$. Thus $g_\parallel - g_0$ can be written as

$$g_\parallel - g_0 = \Delta^2 g_\parallel(\text{CF}) + \Delta^2 g_\parallel(\text{CT}) + \Delta^3 g_\parallel(\text{CF}) + \ldots \tag{3.9}$$

where $\Delta^2 g_\parallel(\text{CF})$ and $\Delta^2 g_\parallel(\text{CT})$ reflect the second-order contributions from the crystal-field and charge-transfer excitations, respectively, and $\Delta^3 g_\parallel(\text{CF})$ corresponds to the third-order contribution coming from crystal-field excitations. The expressions for all these quantities can be found in [32].

In ionic systems like the present ones the first term is clearly dominant. For instance, $\Delta^2 g_\parallel(\text{CF})$ is about 300 times higher than $\Delta^2 g_\parallel(\text{CT})$ and about 15 times higher than $|\Delta^3 g_\parallel(\text{CF})|$ for NiF_6^{5-}. The expression for $\Delta^2 g_\parallel(\text{CF})$ can be written briefly as

$$\Delta^2 g_\parallel(\text{CF}) = (8\xi_M/\Delta_1) f_1(\alpha_0, \alpha_1, \mu_p, \xi_L) \tag{3.10}$$

where the f_1 factor, depending upon MO coefficients of b_{1g}^* and b_{2g}^* levels as well as on the ligand spin–orbit coefficient ξ_L, is less than unity for systems with low covalency. A similar situation is encountered for $g_\perp - g_0$, which is also dominated by the $\Delta^2 g_\perp(\text{CF})$ contribution given by

$$\Delta^2 g_\perp(\text{CF}) = (2\xi_M/\Delta_2) f_2(\alpha_0, \alpha_2, \mu_p, \xi_L) \tag{3.11}$$

where f_2 plays the role of a reduction parameter provided covalency is low. This situation is, however, completely changed when the unpaired electron spends more time on the ligands than on the central ion, as happens for $CdBr_2$:Ag^{2+} [44].

4. Method of analysis

To gain a better insight into the main causes that determine the dependence of energy levels on metal–ligand distances, we have expressed the energy of a given level of the isolated complex as a sum of three contributions, depicted in figure 3. To clarify the ideas, let us first consider a mainly d electronic level, whose wavefunction belongs to the Γ irreducible representation and whose energy is written as $\epsilon_M(\Gamma)$. Once the chemical bond is formed in the complex, the total charges on metal and ligand ions are q_M and q_L, respectively, usually being different from the nominal charges characteristic of isolated ions. From experimental atomic data and also from density-functional calculations, it is possible to determine the energy $\epsilon_d(q_M)$ corresponding to the d level of an *isolated* metal ion *but* with a fractional charge q_M. This quantity $\epsilon_d(q_M)$ (derived from $\text{VSIE}(q_M)$) is the first contribution to $\epsilon_M(\Gamma)$.

The second one arises from the electrostatic interaction of ligand ions with charge q_L upon the electron placed into the d orbital. After this second step $\epsilon_M(\Gamma)$ is thus approximated by

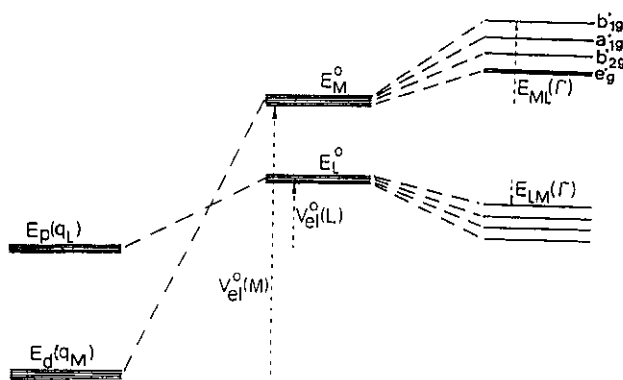$$\epsilon_M^0 = \epsilon_d(q_M) + V_{el}(M). \tag{4.1}$$

Figure 3. Pictorial description of the three contributions to the one-electron energies $\epsilon_M(\Gamma)$ and $\epsilon_L(\Gamma)$. The meaning of symbols is explained in the text.

For an elongated unit like NiF_6^{5-}, $V_{el}(M)$ is well approximated by

$$V_{el}^0(M) = -[4e^2 q_L(1)/R_{eq} + 2e^2 q_L(2)/R_{ax}] \tag{4.2}$$

where $q_L(1)$ and $q_L(2)$ denote the total charge carried by equatorial and axial ligand ions, respectively. In the SCCEH method ϵ_M^0 corresponds to diagonal elements, $h_{MM}(\Gamma)$, arising from the one-electron Hamiltonian of the isolated complex. As the d electron is not located at the centre of the metal ion, there are, however, corrections to $V_{el}^0(M)$. Such corrections are different for $x^2 - y^2$ or xy electrons, for instance, and so they give rise to the purely crystal-field contribution to Δ_1, equal to ~ 1000 cm^{-1} for NiF_6^{5-}. As found for other TM systems, this value is only about 0.2 times the right Δ_1 value, implying that such corrections to $V_{el}^0(M)$ do not play a relevant role at all.

By contrast, the energy difference among the five mainly d orbitals arises essentially from the interaction of a d level, transforming like Γ, with ligand wavefunctions of the same symmetry via the off-diagonal elements of the one-electron Hamiltonian. This interaction, reflecting directly the chemical bond, is also the source of electronic charge transfer between ligands and metal. The contribution to $\epsilon_M(\Gamma)$ due to the last step will be called $\epsilon_{ML}(\Gamma)$ and so

$$\epsilon_M(\Gamma) = \epsilon_d(q_M) + V_{el}(M) + \epsilon_{ML}(\Gamma). \tag{4.3}$$

A similar expression holds for the mainly $n_L p$ ligand orbitals

$$\epsilon_L(\Gamma) = \epsilon_L^0 + \epsilon_{LM}(\Gamma)$$
$$\epsilon_L^0 = \epsilon_p(q_L) + V_{el}(L) \tag{4.4}$$

where $V_{el}(L)$ is rather different from $V_{el}(M)$ and can be taken as

$$V_{el}^0(L) = -[q_M + 1.91 q_L(1) + 2w q_L(2)]e^2/R_{eq}$$
$$w = R_{eq}/(R_{eq}^2 + R_{ax}^2)^{1/2}. \tag{4.5}$$

In practice, the quantities $\epsilon_{ML}(\Gamma)$ and $\epsilon_{LM}(\Gamma)$ are derived from the $\epsilon_M(\Gamma)$ and $\epsilon_L(\Gamma)$ values supplied by the MO calculations using equations (4.3) and (4.5) and the values of the final charges also appearing in the output of calculations. If bonding is rather ionic and there is only one linear combination of atomic orbitals (LCAO) of ligands transforming as Γ, then $\epsilon_{ML}(\Gamma)$ can be approximated as

$$\epsilon_{ML}(\Gamma) \simeq [h_{ML}(\Gamma) - \epsilon_M^0 S_{ML}(\Gamma)]^2/(\epsilon_M^0 - \epsilon_L^0) \tag{4.6}$$

which converts to

$$\epsilon_{ML}(\Gamma) \simeq (\epsilon_L^0)^2 S_{ML}^2(\Gamma)/(\epsilon_M^0 - \epsilon_L^0) \tag{4.7}$$

using the Wolfsberg–Helmholz guess [45]

$$h_{ML}(\Gamma) = (k/2)[h_{MM}(\Gamma) + h_{LL}(\Gamma)] S_{ML}(\Gamma) \tag{4.8}$$

and taking $k = 2$.

The preceding relations are the basis for understanding the dependence of different parameters of NiF$_6^{5-}$ on the two Ni$^+$–F$^-$ distances, as discussed in the next section.

5. Results on Ni$^+$ systems

5.1. Energy levels for NiF$_6^{5-}$: dependence on R_{eq}

The order of levels found in our calculations is that shown in figure 2. Figure 4 depicts the dependence on R_{eq} of three selected one-electron levels: the two antibonding b$_{1g}^*$ and b$_{2g}^*$ and the mainly ligand e$_u(\pi + \sigma, \text{eq})$ ones. It can be noticed, first of all, that the dependence obtained through both methods of calculation is very similar. In fact, both methods indicate that the two mainly d orbitals are much more sensitive than the mainly ligand ones to changes of R_{eq}. More precisely, at $R_{eq} \simeq 210$ pm it is found $\partial\epsilon(\text{b}_{1g}^*)/\partial R_{eq} = -1030$ cm^{-1}/pm, $\partial\epsilon(\text{b}_{2g}^*)/\partial R_{eq} = -880$ cm^{-1}/pm and $\partial\epsilon(\text{e}_u)/\partial R_{eq} = -140$ cm^{-1}/pm. These figures stress that a charge-transfer transition, like e$_u(\pi + \sigma, \text{eq}) \rightarrow$ b$_{1g}^*$, is more sensitive than a crystal-field one, like b$_{2g}^* \rightarrow$ b$_{1g}^*$, to R_{eq} variations. This conclusion has proven to be true in the study of some Cu^{2+} systems having their charge-transfer bands in the optical domain [46, 47]. As regards the dependence of Δ_1 on R_{eq}, it is found that $\Delta_1 \propto R_{eq}^{-n}$ around $R_{eq} = 210$ pm. A value $n = 4.7$ has been derived from MS-$X\alpha$ calculations while $n = 4.4$ has been found through the SCCEH method. The use in the latter method of single-zeta wavefunctions can increase n up to about 8, which is unreliable. In the case of MnF$_6^{4-}$ in fluoroperovskites the exponent n has been measured experimentally [15], being equal to $n = 4.7$. Values lying between 4 and 6 have been calculated for other TM ions in fluorides [11, 48], while the analysis of experimental data of V^{2+}-doped fluoroperovskites [49] are consistent with $n \simeq 5$.

Although for Ni$^+$ systems the optical transitions Δ_1 and Δ_2 have not been measured, experimental evidence on the dependence of Δ_1 and Δ_2 upon R_{eq} is indirectly reached by studying the g-tensor as explained in section 5.5.

The origin of the variations displayed in figure 4 can be understood by looking at figure 5. Such a figure demonstrates that the main source of dependence of
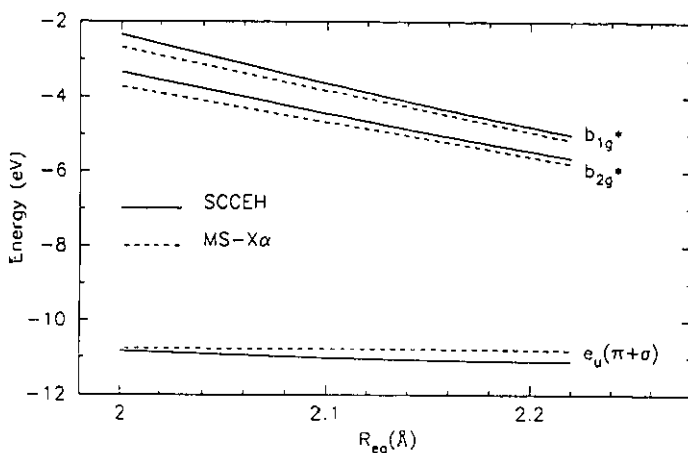
Figure 4. Dependence of one-electron energies of b_{1g}^* ($\sim x^2 - y^2$), b_{2g}^* ($\sim xy$) and $e_u(\pi + \sigma, eq)$ orbitals corresponding to NiF_6^{5-} on R_{eq} derived from MS-$X\alpha$ and SCCEH calculations. Results have been obtained for a $NiLi_{12}F_{14}^-$ cluster. R_{ax} has been taken equal to 243 pm.

the b_{1g}^* level on R_{eq} comes from the $V_{el}(M)$ term. This way, for $R_{eq} = 210$ pm and $R_{ax} = 243$ pm, and taking $q_L(1) = q_L(2) = -1$, from equation (4.2) we have $\partial V_{el}(M)/\partial R_{eq} = -1050$ cm^{-1}/pm, which is comparable to $\partial \epsilon(b_{1g}^*)/\partial R_{eq} = -1030$ cm^{-1}/pm. On the other hand, for the same distances and taking $q_M = +1$, from equation (4.5) we calculate $\partial V_{el}(L)/\partial R_{eq} = -80$ cm^{-1}/pm. Therefore, the very distinct dependence on R_{eq} displayed by the mainly d levels and the mainly ligand level in figure 4 reflects to a great extent that of $V_{el}(M)$ and $V_{el}(L)$, respectively.
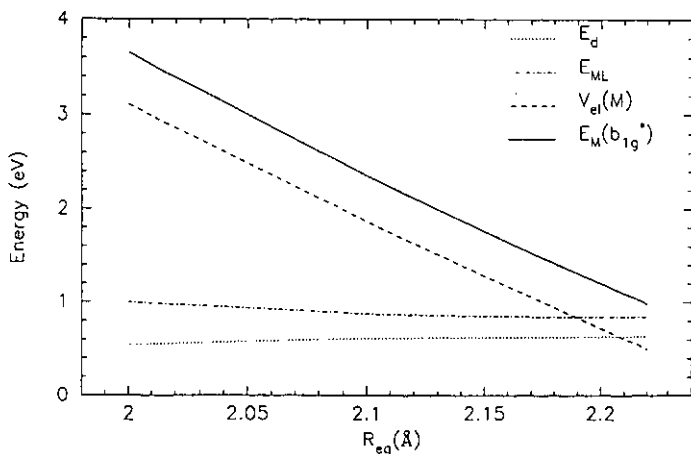

Figure 5. R_{eq} dependence of the three contributions called ϵ_d, $V_{el}(M)$ and ϵ_{ML} to the b_{1g}^* one-electron energy for the elongated NiF_6^{5-} complex. R_{ax} has been taken equal to 243 pm.

Very recently [50] the key role played by an electrostatic contribution like $V_{el}(M)$

and $V_{el}(L)$ for understanding the variations displayed by the charge-transfer gap of insulating cuprates like L_2CuO_4 (L = Pr, Nd, Sm, Eu, Gd), $Bi_2Sr_2YCu_2O_8$ or $YBa_2Cu_3O_6$ has been emphasized.

5.2. Transferred spin densities for NiF_6^{5-}: dependence on R_{eq}

Figure 6 points out that again the results found through the MS-$X\alpha$ and SCCEH methods are rather similar. Both methods reveal a high ionicity of the bonding (f_σ being about 2%) and give f_s values much smaller than those of f_σ. Despite this fact, both methods stress that f_s is, however, much more sensitive to R_{eq} variations than f_σ. The origin of this important feature can simply be explained as follows. If bonding is ionic, the expressions for $\beta_0\mu_p$ and $\beta_0\mu_s$ can be approximated, assuming the Wolfsberg–Helmholz guess (equation (4.8)) and $k = 2$, as

$$\beta_0\mu_p = -\epsilon_L^0(2p)S_{p\sigma}/[\epsilon_M^0 - \epsilon_L^0(2p)]$$

$$\beta_0\mu_s = -\epsilon_L^0(2s)S_s/[\epsilon_M^0 - \epsilon_L^0(2s)]. \tag{5.1}$$
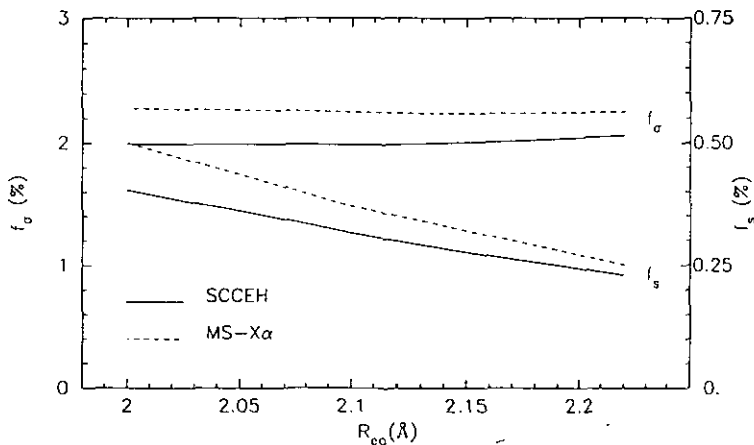

Figure 6. R_{eq} dependence of the f_σ and f_s transferred spin densities obtained for the elongated NiF_6^{5-} complex ($R_{ax} = 243$ pm) through MS-$X\alpha$ and SCCEH methods.

As the 2s orbital of fluorine is much more internal than the 2p one, S_s is more sensitive to R_{eq} changes than $S_{p\sigma}$. Quantitatively, $S_{p\sigma} \propto R_{eq}^{-\gamma_p}$ with $\gamma_p = 2.0$ while $S_s \propto R_{eq}^{-\gamma_s}$ with $\gamma_s = 3.5$ for NiF_6^{5-}. Nevertheless, when R_{eq} decreases, ϵ_M^0 also increases, which in turn produces an increase of $\epsilon_M^0 - \epsilon_L^0(2p)$, tending to cancel the increase of the overlap integral $S_{p\sigma}$. More precisely, $[\epsilon_M^0 - \epsilon_L^0(2p)] \propto R_{eq}^{-\gamma_c}$ with $\gamma_c \simeq 2.0$. Thus, this simple scheme is able to explain why the covalency parameter f_σ can remain almost constant when R_{eq} decreases, although the charge-transfer transitions can be quite sensitive to that change.

As $\epsilon_L^0(2p) - \epsilon_L^0(2s) \simeq 25$ eV for fluorine, the relative variations undergone by $\epsilon_M^0 - \epsilon_L^0(2s)$ are much less important than those of $\epsilon_M^0 - \epsilon_L^0(2p)$. In other words, $\epsilon_M^0 - \epsilon_L^0(2s)$ is practically independent of R_{eq} and so f_s follows the behaviour of $S_s^2(R_{eq})$, thus explaining the sensitivity of f_s to R_{eq} changes.

The dependence of f_s on R_{eq} can be well fitted through the law

$$\beta_0 \mu_s = c S_s(R_{eq}) \tag{5.2}$$

where c is a constant. Since the first study carried out for Mn^{2+} in fluorides [13], a law of this kind has been found for systems involving unpaired electrons with σ character [7, 51].

5.3. The superhyperfine tensor: determination of R_{eq}

Through the preceding results on NiF_6^{5-} and equations (3.6) and (3.7), it is simple to predict the dependence of A_{an} and A_s on R_{eq}. For $R_{eq} = 210$ pm and taking $f_\sigma = 2.2\%$ it is found that $A_\sigma = 10.4 \times 10^{-4}$ cm^{-1} and $A_d = 2.7 \times 10^{-4}$ cm^{-1}.

Therefore, A_{an} would be clearly dominated by the A_σ contribution and thus it is practically independent of R_{eq}. These theoretical conclusions thus explain reasonably well why the experimental A_{an} value of centre I in several fluoroperovskites is the same, within experimental uncertainty, as pointed out in table 1. At the same time, the theoretical value $A_{an} = 13.1 \times 10^{-4}$ cm^{-1} computed for $R_{eq} = 210$ pm is not far from the experimental value corresponding to centre I in fluoroperovskites.

Having in mind the strong dependence on R_{eq} shown by f_s in figure 6 and the relation between A_s and f_s displayed by equation (3.5), the changes experienced by A_s when the host lattice is changed can also reasonably be understood only on the basis of different R_{eq} values reached by the NiF_6^{5-} complex in different fluoroperovskites. Equation (5.2) allows one to determine the true R_{eq} value provided we know the right value of the constant c. In the case of MnF_6^{4-} this constant has been derived from the analysis of experimental results on several fluoroperovskites [13] and is equal to $c = 1.27$. This figure has to be compared with the theoretical values reached through Hartree–Fock–Roothaan [7] ($c = 1.23$) and SCCEH [52] ($c = 1.42$) calculations. For NiF_6^{5-}, SCCEH calculations give $c = 1.3$ while Hartree–Fock–Roothaan calculations for monovalent ions (Cr^+, Ni^+, Fe^+) in fluorides [51] give c values lying between 1.1 and 1.2. Here we shall assume $c = 1.1$, following the work of [28], for deriving the R_{eq} values shown in table 1 from the corresponding A_s. It is important to remark, however, that this assumption has practically no influence on the *differences* of R_{eq} corresponding to a given centre but placed in two different host lattices. This way, if it is assumed that $c = 1.2$, the R_{eq} values for centre I in $KMgF_3$ and K_2MgF_4 would be equal to $R_{eq} = 219$ pm and $R_{eq} = 215$ pm, respectively, the difference between them being equal to 4 pm as in table 1.

The values of R_{eq} collected in table 1 for centre I in different fluoroperovskites are ordered following the corresponding values of R_0, where R_0 denotes the metal–ligand distance for the perfect undistorted lattice. This behaviour, which has been found for other impurities [16, 53], reflects the important influence of the rest of the lattice upon the equilibrium distance of the complex. It is worth noting that a change of R_0, ΔR_0, due to the host–lattice change, produces a change of R_{eq}, ΔR_{eq}, that is clearly smaller. To make this idea more precise, let us define the f factor as

$$f = \Delta R_{eq} / \Delta R_0. \tag{5.3}$$

From the data of table 1 for centre I it is found that $f = 0.33 \pm 0.08$. This figure has to be compared with the value $f = 0.32 \pm 0.05$ derived from Mn^{2+} in

fluoroperovskites [16], where it reflects the tendency of the impurity to get a metal–ligand distance as close as possible to the sum of ionic radii of Mn^{2+} and F^-.

Equation (5.2) for the present case means that f_s and A_s are determined to a great extent only by the overlap integral $S_s(R_{eq})$. We have applied the same equations and assumed $c = 1.1$ to derive the R_{eq} values for centres II and III, which are also collected in table 1. The same procedure is employed for Ni^+ centres in CaF_2 and SrF_2 and the corresponding R_{eq} values are given in table 2. The results are reasonable as R_{eq} decreases on going from centre I to centre III for every host lattice, this behaviour being in agreement with the expected decrease of R_{eq} when the coordination number decreases [54].

5.4. Influence of axial ligands

Table 3 compares the theoretical results obtained for NiF_6^{5-} and NiF_4^{3-} at the *same* $R_{eq} = 213$ pm value. When the two axial ligands are removed, the trends obtained through the SCCEH and MS-$X\alpha$ methods are again quite similar. The main features of the results (displayed in table 3) on passing from NiF_6^{5-} to NiF_4^{3-}, keeping the same R_{eq} value are

(i) Δ_1 experiences a slight increase. It is worth noting that Δ_1 should not change in a pure crystal-field description.

(ii) The change experienced by Δ_2 is higher than that of Δ_1.

(iii) The charge-transfer transition $e_u(\pi + \sigma, eq) \rightarrow b_{1g}^*$ undergoes a decrease of about 15 000 cm^{-1}.

(iv) f_σ is sensitive to the presence of axial ligands.

The increase of f_σ on passing from NiF_6^{5-} to NiF_4^{3-} keeping R_{eq} constant (table 3) can be related to the increase experienced by A_{an} on going from centre I to centre III in table 1, which is about 3×10^{-4} cm^{-1}. Quantitatively, if $f_\sigma = 2.2\%$ for NiF_6^{5-} and $f_\sigma = 3.5\%$ for NiF_4^{3-}, this would lead to an increase of A_{an}, $\Delta A_{an} \simeq 6 \times 10^{-4}$ cm^{-1}, which seems to be higher than the experimental value. In other words, the experimental results of table 1 are more consistent, through equations (3.6) and (3.7), with f_σ values of 2% and 2.5% for NiF_6^{5-} and NiF_4^{3-}, respectively, and so, although the trend found through both methods is correct, the MS-$X\alpha$ and specially the SCCEH method lead to an overestimation of the f_σ increase on passing from NiF_6^{5-} to NiF_4^{3-}.

Table 3. Comparison between theoretical values obtained for NiF_6^{5-} ($R_{ax} = 243$ pm) and NiF_4^{3-} at the same distance $R_{eq} = 213$ pm. First and second rows give MS-$X\alpha$ and SCCEH results, respectively. Δ_1 and Δ_2 denote the energies of the crystal-field transitions $b_{2g}^* \rightarrow b_{1g}^*$ and $e_g^* \rightarrow b_{1g}^*$, respectively, while E_u means the charge transfer transition $e_u(\pi + \sigma, eq) \rightarrow b_{1g}^*$. Values of Δ_1, Δ_2 and E_u are given in cm^{-1} and f_σ in %.

System	Δ_1	Δ_2	E_u	f_σ
NiF_6^{5-}	6410	7010	69 690	2.24
	6070	6850	56 860	1.99
NiF_4^{3-}	7610	8450	56 770	3.49
	7200	9280	41 090	3.88

As regards f_s the SCCEH calculations indicate that the decrement undergone on going from NiF_4^{3-} to NiF_6^{5-} is about 15% and thus much smaller than that corresponding to f_σ. This fact and the overestimation made by calculations on f_σ both support that the constant c can indeed be the same for NiF_6^{5-} and NiF_4^{3-} as was taken in section 5.3.

Qualitatively, the removal of two axial ligands keeping the same R_{eq} value decreases the $\epsilon_M^0 - \epsilon_L^0$ quantity, mainly because of the involved diminution of electrostatic repulsion on 3d electrons, termed V_M. This decrement clearly favours smaller energies for the charge-transfer transitions, although at the same time inducing higher values of the positive ϵ_{ML} contribution to $\epsilon_M(\Gamma)$, as pointed out by equation (4.6). This increase of ϵ_{ML} tends to cancel, but only partially, the effects of the diminution of $\epsilon_M^0 - \epsilon_L^0$. As an example, taking $q_M = 1$ and $q_L(1) = q_L(2) = -1$, the removal of two axial ligands at $R_{ax} = 240$ pm would imply a variation $\delta(\epsilon_M^0 - \epsilon_L^0) = \delta(V_M - V_L) = -37000$ cm^{-1}, while the calculated diminution of the $e_u(\pi + \sigma, eq) \rightarrow b_{1g}^*$ charge-transfer transition is only about 15000 cm^{-1}. The increase undergone by the $\epsilon_{ML}(\Gamma)$ quantity on passing from NiF_6^{5-} to NiF_4^{3-} keeping R_{eq} constant increases the difference $\epsilon_M(\Gamma_1) - \epsilon_M(\Gamma_2)$ corresponding to two mainly 3d orbitals with different symmetry. This simple idea thus explains why Δ_1 can increase although R_{eq} is kept constant.

In the case of Δ_2 the removal of axial ligands produces an additional effect giving rise to a higher increase than that experienced by Δ_1. In fact, such a removal destroys the admixture of axial ligand wavefunctions like $|p_x(5)\rangle$, $|p_x(6)\rangle$, etc., in the antibonding e_g^* orbital. As in an antibonding orbital the interaction (via the off-diagonal elements of h) with ligand orbitals gives rise to an increase of its energy, the suppression of bonding with axial ligands decreases the energy of the e_g^* orbital and consequently increases Δ_2. The experimental verification of the present conclusions upon the influence of axial ligands on Δ_1 and Δ_2 is obtained, though indirectly, from the g-tensor study reported in section 5.5. Although charge-transfer transitions for Ni^+ in fluorides have not been detected experimentally, the present trends are of great interest for understanding the experimental data of systems involving $CuCl_6^{4-}$ and $CuCl_4^{2-}$ complexes, as discussed in section 6.

5.5. The g-tensor of Ni$^+$ centres

We have calculated the dependence of $g_\parallel$ and $g_\perp$ on R_{eq} for both NiF_6^{5-} and NiF_4^{3-} complexes from the MO coefficients obtained through our SCCEH and MS-$X\alpha$ calculations and the general expressions reported in [32] and discussed in section 3.3. The results are collected in figures 7 and 8, where they are directly compared to the experimental values of Ni^+ centres in fluoroperovskites and in CaF_2 and SrF_2. For achieving that comparison, the R_{eq} value for each case is that derived from the experimental A_s, as indicated in section 5.3. Having in mind that our calculation of the g-tensor *does not involve adjustable parameters*, we find that the main features displayed by the experimental g-tensor of all Ni^+ centres can reasonably be understood through the present theoretical results on NiF_6^{5-} and NiF_4^{3-} complexes. Again, both methods of calculation lead to the same trends. This way, the increase undergone by the $g_\parallel$ factor of a given centre through the series $K_2MgF_4 \rightarrow KMgF_3 \rightarrow RbCaF_3$ can mainly be ascribed to the increase experienced by R_{eq}, previously known from the analysis of experimental A_s data. Another important feature encountered in the present calculations, which is also in agreement with

experimental data, concerns the comparison of the plots $g_{\parallel}(R_{eq})$ and $g_{\perp}(R_{eq})$ for centres I and III. It can be seen that $g_{\parallel}(R_{eq})$ and especially $g_{\perp}(R_{eq})$ for centre I lie above the corresponding plots of centre III, while the results corresponding to centre II lie in an intermediate region.
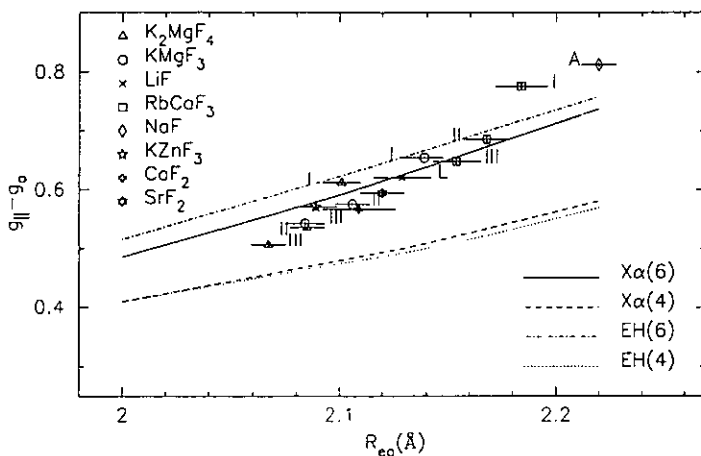

Figure 7. R_{eq} dependence of theoretical $g_{\parallel} - g_0$ value derived from SCCEH and MS-$X\alpha$ calculations and the expressions of [32] for NiF$_6^{5-}$ ($R_{ax} = 243$ pm) and NiF$_4^{3-}$ complexes. Experimental values corresponding to Ni⁺ centres I, II and III in fluoroperovskites as well as to Ni⁺ centres in CaF$_2$, SrF$_2$, LiF and NaF are included for comparison. The R_{eq} value for these systems was derived from the experimental A_s quantity as explained in section 5.3.
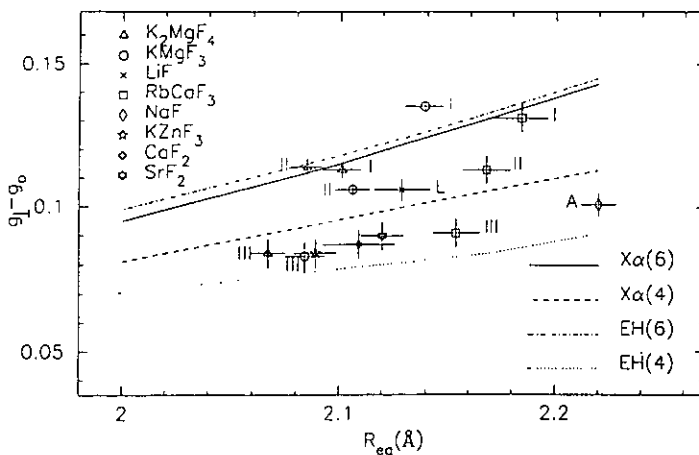

Figure 8. The same as for figure 7 but for $g_{\perp} - g_0$.

As regards Ni⁺ centres observed in CaF$_2$ and SrF$_2$, figure 8 shows that their experimental $g_{\perp}$ values are quite comparable to those found for Ni⁺ (III) centres

in fluoroperovskites. This is a quite reasonable result, as the local geometry of Ni^+ centres in CaF_2 and SrF_2 is very close to that of a square-planar NiF_4^{3-} complex [22, 23].

In the present cases the dependence of $g_\parallel - g_0$ and $g_\perp - g_0$ upon R_{eq} mimics to a great extent that of Δ_1^{-1} and Δ_2^{-1}, respectively. This can be seen in figure 9, where the calculated product $(g_\parallel - g_0)\Delta_1$ experiences a variation of only $\sim 5\%$ in the range 200 pm $< R_{eq} <$ 220 pm. This important result, already suggested in the analysis of experimental data of Ni^+ centres in alkali fluorides [28], is a direct consequence of the significant ionicity present in NiF_6^{5-} and NiF_4^{3-} complexes as well as of the very slight dependence of f_σ and α_0^2 upon R_{eq} discussed in section 5.2. Now, taking into account this fact, it is quite simple to understand why $g_\perp - g_0$ is more sensitive than $g_\parallel - g_0$ for distinguishing a centre I from a centre III only through the experimental g-tensor. Indeed, this feature, well shown in figures 7 and 8, directly reflects the higher sensitivity of Δ_2, compared to that of Δ_1, to the removal of axial ligands as explained in detail in section 5.4.
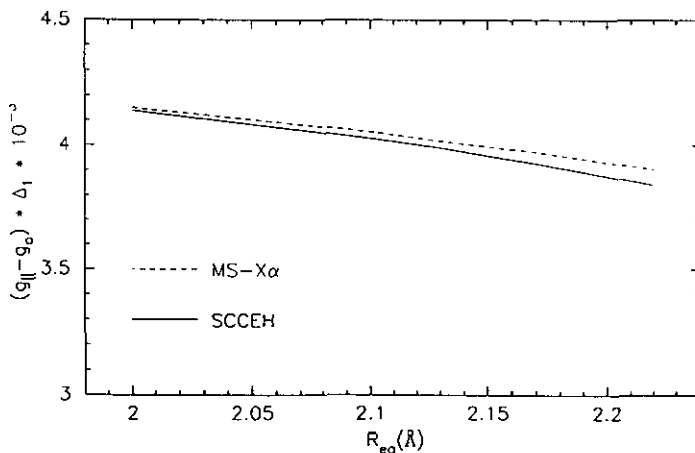

Figure 9. R_{eq} dependence of the product $(g_\parallel - g_0)\Delta_1$ calculated through MS-$X\alpha$ and SCCEH methods for the elongated NiF_6^{5-} complex.

Before ending this section, let us mention other important consequences contained in figures 7 and 8:

(i) The Ni^+ centre discovered in $KZnF_3$ should correspond to a Ni^+ (III) centre involving two axial vacancies, and not one as was supposed by Rousseau *et al* [21] in the first published work on Ni^+ in fluoroperovskites.

(ii) The so-called A centre found by Hayes and Wilkens [31] in $NaF:Ni^+$ can hardly be associated with a pure NiF_6^{5-} complex with elongated octahedral geometry.

(iii) Finally, the results of figure 7 point out that, for the present cases, variations ΔR_{eq} certainly smaller than 1 pm can be measured by looking only at the experimental $g_\parallel$ value. More precisely, if the uncertainty in $g_\parallel$ is 0.002, variations $|\Delta R_{eq}| \geqslant 0.3$ pm produced by external pressures could be followed through the variations of the experimental $g_\parallel$ factor.

6. Survey of Cu^{2+} and Ag^{2+} systems

Once the salient features displayed by the experimental parameters of the simple Ni$^+$ centres found in fluoroperovskites as well as in other fluoride materials have all reasonably been understood through the present analysis, it appears as a good challenge to investigate whether the theoretical results on Ni$^+$ complexes can serve as a *guide* for explaining the main trends displayed by experimental data of other more covalent d^9 systems. In particular, it is attractive to study systems for which the charge-transfer transitions have been measured.

For Ni$^+$ in fluorides, such transitions would lie in the vacuum-ultraviolet region (figure 4) and because of this they have not been detected up to now. The present section will be mainly devoted to analysing results coming from tetragonal Cu^{2+} centres in chlorides, for the following reasons:

(i) Both the elongated CuCl$_6^{4-}$ and the pure square-planar complex have been observed in different crystalline matrices. This way the CuCl$_6^{4-}$ complex is formed [55–60] in Cu^{2+}-doped CdCl$_2$, LiCl and NaCl, while the CuCl$_4^{2-}$ unit is found [61] in K$_2$PdCl$_4$:Cu^{2+} and also in some pure compounds [62–64] like (N-mpH)$_2$CuCl$_4$, (creat)$_2$CuCl$_4$, etc. (Here N-mpH and creat stand for *N*-methylphenethylammonium and creatininium, respectively.)

(ii) The charge-transfer transitions of both species have been well measured [55, 56, 59, 62] in the optical domain as could be expected from the optical electronegativity scale. It is worth noting that the optical electronegativity $\chi = 2.4$ associated [65] with Cu^{2+} is the highest among the divalent 3d ions, while that for Ni$^+$ has been estimated [29] to be $\chi < 1.8$. In the case of Ag^{2+}, χ is equal [66] to 2.8, but optical experimental results on this impurity are more scarce than for Cu^{2+}.

In table 4 are compared the experimental optical [55, 56] and EPR results [57] for CdCl$_2$:Cu^{2+} with the optical results [62, 63] for (N-mpH)$_2$CuCl$_4$ and the EPR results [61] of K$_2$PdCl$_4$:Cu^{2+}. The last system is the only one involving a square-planar CuCl$_4^{2-}$ unit in which Cu^{2+} appears as impurity and, therefore, it is the only one in which the SHF tensor has been measured. It is worth noting, however, that $g_\parallel = 2.221 \pm 0.004$ and $g_\perp = 2.040 \pm 0.004$ have been measured [64] for (N-mpH)$_2$CuCl$_4$ and thus they are quite close to the values measured for CuCl$_4^{2-}$ in K$_2$PdCl$_4$.

Table 4. Representative values of some experimental optical and EPR parameters for CuCl$_6^{4-}$ and CuCl$_4^{2-}$ complexes. The values given for CuCl$_6^{4-}$ all refer to CdCl$_2$:Cu^{2+} [55–57]. EPR and optical parameters of CuCl$_4^{2-}$ correspond to K$_2$PdCl$_4$:Cu^{2+} [61] and (N-mpH)$_2$CuCl$_4$ [62, 63], respectively. Δ_1, Δ_2 and E_u are given in cm^{-1}, while A_s and A_{an} are in 10^{-4} cm^{-1} units.

Complex	Δ_1	Δ_2	E_u	$g_\parallel - g_0$	$g_\perp - g_0$	A_s	A_{an}
CuCl$_6^{4-}$	9437	10970	25510	0.34	0.073	10.0	4.3
CuCl$_4^{2-}$	12480	14625	26050	0.23	0.047	11.5	5.2

First of all it can be seen in table 4 that A_s is higher for K$_2$PdCl$_4$:Cu^{2+} than for CdCl$_2$:Cu^{2+}, pointing out that R_{eq} is in fact higher for the latter than for the former system. This is in qualitative agreement with the finding for Ni$^+$ centres and the

general relation existing between metal–ligand distances and coordination number. The analysis of experimental data carried out in [32] shows that the difference of R_{eq} between both systems is about 7 pm. The other data displayed in table 4 exhibit the same behaviour found in the comparison between NiF_6^{5-} and NiF_4^{3-} with the apparent exception of E_u. This way Δ_1, Δ_2 and A_{an} experience a significant increase on passing from $CuCl_6^{4-}$ to $CuCl_4^{2-}$ while $g_\parallel - g_0$ decreases. By contrast E_u is practically the same for $CdCl_2$:Cu^{2+} and for $(N\text{-mpH})_2CuCl_4$. To understand this apparently puzzling feature, it is necessary to remark that the experimental data of both systems *do not correspond to the same R_{eq}* value because of the different number of Cl^- ligands. The calculation of the total variation, δE, experienced by an optical transition on passing from the first system to the second one can be done through the following two steps: (i) In the first step, the R_{eq} distance of the $CuCl_6^{4-}$ complex undergoes a change $\delta_1 R_{eq} \simeq -7$ pm while R_{ax} is kept constant. This induces a change termed $\delta_1 E$ upon the optical transition. For Ni^+ systems both $\delta_1 \Delta_1$ and $\delta_1 E_u$ are positive. (ii) Once the equatorial equilibrium distance of the square-planar unit is reached, the two axial ligands are removed keeping R_{eq} constant. This gives rise to a second change, $\delta_2 E$, on the optical transition. For Ni^+ systems $\delta_2 \Delta_1$ is also positive *but* $\delta_2 E_u$ is negative.

The total energy δE for an isolated complex is just $\delta_1 E + \delta_2 E$ and so the experimental value of Δ_1 should be higher for $CuCl_4^{2-}$ than for $CuCl_6^{4-}$ provided the trends for Ni^+ are followed, as indeed is found (table 4). Furthermore, the present arguments suggest that δE_u could be practically zero although $\delta\Delta_1$ and $\delta\Delta_2$ are positive. From a quantitative point of view if $\delta R_{eq} \simeq -7$ pm and $\partial E_u / \partial R_{eq} \simeq -700$ cm^{-1}/pm [43], then $\delta_1 E_u \simeq +5000$ cm^{-1}. Now if we assume that E_u decreases about 20% upon removal of axial ligands, as for Ni^+ centres, this would lead to $\delta_2 E_u \simeq -5000$ cm^{-1}, so δE_u could in fact be close to zero on passing from $CdCl_2$:Cu^{2+} to $(N\text{-mpH})_2CuCl_4$. Also, a simple analysis of the experimental $\delta\Delta_1$ and $\delta\Delta_2$ quantities reveals that such variations cannot be understood only through the decrease undergone by R_{eq}. In fact, assuming that both Δ_1 and Δ_2 are roughly proportional to R_{eq}^{-5} and that $\delta R_{eq} = -7$ pm, we get $\delta_1 \Delta_1 = 1500$ cm^{-1} and $\delta_1 \Delta_2 = 1900$ cm^{-1}. Such values are clearly smaller than the experimental variations $\delta\Delta_1 = 3043$ cm^{-1}, $\delta\Delta_2 = 3655$ cm^{-1} and are thus compatible with $\delta_2 \Delta_1 \simeq 1500$ cm^{-1} and $\delta_2 \Delta_2 \simeq 1800$ cm^{-1}.

In the case of $LiCl$:Cu^{2+}, a $CuCl_6^{4-}$ complex is also formed, although E_u is found [58, 59] to be equal to $28\,000$ cm^{-1}, so it lies about 2500 cm^{-1} higher than the corresponding transition [55] in $CdCl_2$:Cu^{2+}. This blue shift is, however, quite logical if we take into account that R_0 is equal to 274 and 257 pm for $CdCl_2$ and $LiCl$, respectively, and use the results found for Ni^+ and Mn^{2+} centres in fluorides [16]. In these cases the R values are different from the corresponding R_0 values but they are ordered in the same way. Quantitatively, accepting [46] that $\partial E_u / \partial R_{eq} = -700$ cm^{-1}/pm, the 2500 cm^{-1} shift found on passing from $CdCl_2$:Cu^{2+} to $LiCl$:Cu^{2+} is compatible with a variation $\Delta R_{eq} \simeq -3.5$ pm, implying that $R_{eq} \simeq 231$ pm for $CuCl_6^{4-}$ in $LiCl$. This value is still higher than $R_{eq} = 226.5$ pm and $R_{eq} = 225.1$ pm corresponding to $(N\text{-mpH})_2CuCl_4$ and $(creat)_2CuCl_4$, where a $CuCl_4^{2-}$ unit is involved [62, 63].

In the case of $SrCl_2$:Cu^{2+} the EPR results [24] show that Cu^{2+} is surrounded by four nearest Cl^- anions displaying an almost D_{4h} geometry. Having in mind the

results on Ni$^+$ centres it could be expected that the spin-Hamiltonian parameters of SrCl$_2$:Cu^{2+} are closer to those of K$_2$PdCl$_4$:Cu^{2+} than to those of CdCl$_2$:Cu^{2+}, as is found. This way $g_{\parallel} = 2.236$ and $g_{\perp} = 2.040 (\pm 0.002)$ are measured [24] for SrCl$_2$:Cu^{2+}, supporting that the Cu^{2+} centre in SrCl$_2$ can essentially be described as being a CuCl$_4^{2-}$ unit.

Let us say a few words about Ag^{2+} in fluorides. In the case of AgSnF$_6$ and AgZrF$_6$ compounds [67], Ag^{2+} is surrounded by an elongated octahedron of F$^-$ ions, a fact that is confirmed by the experimental g-tensor measured by EPR. For AgSnF$_6$ it is found [67] at room temperature that $g_{\parallel} = 2.61$ and $g_{\perp} = 2.15$. The analysis of these values carried out by Friebel [67] leads to a value $f_1 \simeq 0.7$, implying a moderate covalency for the distorted AgF$_6^{4-}$ unit (the factor f_1 is defined in (3.10)). Therefore, we can expect a decrease of both $g_{\parallel}$ and $g_{\perp}$ on going from AgF$_6^{4-}$ to AgF$_4^{2-}$ mainly associated with the expected increase of Δ_1 and Δ_2, respectively. Recently [68] EPR results on BaF$_2$:Ag^{2+} demonstrated that, as found for Cu^{2+} and Ag^{2+} in SrCl$_2$, as well as for Ni$^+$ in CaF$_2$ and SrF$_2$, Ag^{2+} is surrounded by four F$^-$ ions displaying an almost local D$_{4h}$ geometry. The reported $g_{\parallel} = 2.460$ and $g_{\perp} = 2.084 \pm 0.001$ values are clearly smaller than those found for AgSnF$_6$ and thus are consistent with the formation of AgF$_4^{2-}$ units in BaF$_2$. Unfortunately, the optical spectrum of BaF$_2$:Ag^{2+} has not been reported and thus a direct comparison with the crystal-field transitions [67] of AgSnF$_6$ still cannot be carried out.

As remarked through the present work the dependence of $g_{\parallel}$ and $g_{\perp}$ on R_{eq} follows mainly that of Δ_1^{-1} and Δ_2^{-1}, respectively, provided covalency is not too high. In the case of the elongated AgCl$_6^{4-}$ complex, however, it has been shown [66] that $f_{\sigma} = 18\%$ and thus the unpaired electron spends more time on ligands than on silver. Furthermore, related to this strong covalency, it has been demonstrated [66] that the $\Delta^2 g_{\parallel}$(CT) contribution is as important as $\Delta^2 g_{\parallel}$(CF), and thus the explanation about the origin of $g_{\parallel} - g_0$ and its dependence on R_{eq} is certainly more complex than for much more ionic systems. Related to this fact, let us mention that the experimental values of $g_{\parallel}$ for NaCl:Ag^{2+} ($R_0 = 282$ pm) and RbCl:Ag^{2+} ($R_0 = 329$ pm) are equal to 2.198 ± 0.001 and 2.191 ± 0.001, respectively [69]. This behaviour is opposite to that displayed by a given Ni$^+$ centre through the series of fluoroperovskite host lattices and also to that found when comparing $g_{\parallel} = 2.335$ found [57] for CdCl$_2$:Cu^{2+} ($R_0 = 274$ pm) with $g_{\parallel} = 2.373$ measured [60] for NaCl:Cu^{2+} ($R_0 = 282$ pm). As the latter systems both involve the elongated CuCl$_6^{4-}$ unit, which exhibits a moderate covalency ($f_{\sigma} = 9\%$), the $g_{\parallel} - g_0$ values are clearly dominated by the $\Delta^2 g_{\parallel}$(CF) contribution as demonstrated in [32]. Therefore, the increase of $g_{\parallel}$ on going from CdCl$_2$:Cu^{2+} to NaCl$_2$:Cu^{2+} would again reflect a decrease of Δ_1 induced by the expected increase of R_{eq}, following the corresponding R_0 values of the host lattices. Nevertheless, direct checking of this conclusion is not possible as data on the crystal-field spectrum of NaCl:Cu^{2+} are not yet available.

7. Final remarks

The present work shows that the properties due to Ni$^+$(I) and Ni$^+$(III) centres in fluorides can reasonably be explained only through the simple NiF$_6^{5-}$ and NiF$_4^{3-}$ complexes, respectively. The changes experienced by the EPR parameters of a given centre on passing from a lattice to another one essentially reflect the R_{eq} variation

following the change in the chemical pressure exerted by the host lattice upon the complex. Spin-Hamiltonian parameters like A_s or $g_\parallel$ and optical parameters like E_u or Δ_1 have been found to be specially sensitive to R_{eq} changes, ΔR_{eq}, a fact that allows one to measure ΔR_{eq} values well below the limit reached through EXAFS, which is about 2 pm. As the use of the electron nuclear double resonance (ENDOR) technique [70, 71] gives rise to an accuracy of about 10^{-2} G in the measured A_s values, this would allow one to detect ΔR_{eq} values down to about 0.01 pm, taking into account that $\partial A_s / \partial R_{eq} = 1.9$ G/pm, as derived from the present results on Ni^+ centres. Only in the case of CaF_2:Ni^+ have ENDOR measurements been reported [71] although the SHF tensor of the first fluorine shell has not been determined.

It is worth noting that the conclusions reached here are based on theoretical calculations where nuclei are kept frozen and thus dynamical effects are ignored. Dynamical contributions to energy levels arise from zero-point effects or from electron–phonon coupling (in second-order perturbations), which are responsible [72] for isotopic shifts in optical spectra [73]. Also the phonon assistance to parity-forbidden transitions belongs to this kind of effect. Such contributions to the energy of optical transitions are, however, of the order of 500 cm^{-1} or less. Thus it can reasonably be said that the right value of $\partial M / \partial R$ (where M is an EPR or optical parameter) can be *mainly* accounted for through the electronic Hamiltonian with frozen nuclei as is supported by the present results and the preceding ones on Mn^{2+} impurity. Nevertheless, a very precise determination of ΔR from variations of EPR and optical parameters would require a further investigation on dynamical effects as well as on the possible small influences arising from the rest of the lattice.

The results obtained here stress that the main effects arising from *axial vacancies* involved in centres II and III on the electronic properties are: (i) the diminution of the electrostatic repulsion $V_M(el)$; (ii) the breaking of bonds with axial ligands, which is relevant *only* for *some* orbitals, like e_g^* or a_{1g}^*, but unimportant for other ones, like b_{1g}^* or b_{2g}^*; and (iii) the decrease experienced by R_{eq} as a consequence of the coordination number diminution.

As a consequence of this analysis, it has been shown that the g-tensor alone conveys useful information on the presence or absence of axial ligands. It is important to remark that this conclusion, as well as the other ones reached in the study of Ni^+ centres, is useful for understanding the main trends displayed by the experimental results of other d^9 systems with moderate covalency. The validity of this idea has been verified for Cu^{2+} in chlorides and Ag^{2+} in fluorides, whose available EPR and optical data have been well correlated with the number of nearest neighbours and the estimated metal–ligand distances. Further experimental and theoretical work on d^9 impurities is, however, desirable for a more critical examination of the present conclusions.

Very recently data on the distorted AgF_6^{4-} complex in NaF have been reported by Monnier *et al* [74]. The experimental $g_\parallel - g_0 = 0.516$ and $g_\perp - g_0 = 0.094$ values are, respectively, 13% and 16% *higher* than the values found [68] for AgF_4^{2-} in BaF_2. These figures are similar to those obtained in the comparison of the $[g]$ tensor corresponding to $Ni^+(I)$ and $Ni^+(III)$ centres placed in the same fluoroperovskite.

References

[1] Sugano S and Shulman R G 1963 *Phys. Rev.* **130** 517
[2] Adachi H, Shiokawa S, Tsukada M, Satoko C and Sugano S 1979 *J. Phys. Soc. Japan* **47** 1528
[3] Emery J and Fayet J C 1982 *Solid State Commun.* **42** 683
[4] Johansen H and Andersen N K 1986 *Mol. Phys.* **58** 965
[5] Flórez M, Seijo L and Pueyo L 1986 *Phys. Rev.* B **34** 1200
[6] Daul C and Goursot A 1986 *Int. J. Quantum Chem.* **29** 779
[7] Barriuso M T, Aramburu J A, Moreno M, Flórez M, Fernández Rodrigo G and Pueyo L 1988 *Phys. Rev.* B **38** 4239
[8] Winter N W and Pitzer M 1988 *J. Chem. Phys.* **89** 446
[9] Luaña V and Pueyo L 1989 *Phys. Rev.* B **39** 11093
[10] Richardson J W and Janssen G J M 1989 *Phys. Rev.* B **39** 4958
[11] Luaña V, Bermejo M, Flórez M, Recio J M and Pueyo L 1989 *J. Chem. Phys.* **90** 6409
[12] McClure D S and Weaver S C 1991 *J. Phys. Chem. Solids* **52** 81
[13] Barriuso M T and Moreno M 1984 *Phys. Rev.* B **29** 3623
[14] Rodríguez F and Moreno M 1986 *J. Chem. Phys.* **84** 692
[15] Rodríguez F, Moreno M, Tressaud A and Chaminade J P 1987 *Cryst. Latt. Def. Amorph. Mater.* **16** 221
[16] Moreno M 1990 *J. Phys. Chem. Solids* **51** 835
[17] Ham F S 1972 *Electron Paramagnetic Resonance* ed S Geshwind (New York: Plenum) p 1
[18] Zorita E, Alonso P J and Alcala R 1987 *Phys. Rev.* B **35** 3116
[19] Alcala R, Zorita E and Alonso P J 1988 *J. Phys. C: Solid State Phys.* **21** 461
[20] Alcala R, Zorita E and Alonso P J 1988 *Phys. Rev.* B **38** 11156
[21] Rousseau J J, Binois M and Fayet J C 1974 *C. R. Acad. Sci. Paris* B **278** 1079
[22] Casas González J, den Hartog H W and Alcala R 1980 *Phys. Rev.* B **21** 3826
[23] Alonso P J, Casas González J, den Hartog H W and Alcala R 1983 *Phys. Rev.* B **27** 2722
[24] Bill H 1973 *Phys. Lett.* A **44** 101
[25] Bill H, Milleret C and Lacroix R 1973 *Proc. XVII Congress Ampere* ed V Hovi (Amsterdam: North-Holland) p 233
[26] Moreno M 1974 *An. Física* **70** 261
[27] Pierloot K, Van Praet E and Vanquickenborne L G 1992 *J. Chem. Phys.* **96** 4163
[28] Barriuso M T and Moreno M 1984 *Solid State Commun.* **51** 335
[29] Moreno M, Aramburu J A and Barriuso M T 1986 *J. Phys. C: Solid State Phys.* **19** L315
[30] Barriuso M T, Aramburu J A and Moreno M 1990 *J. Phys.: Condens. Matter* **2** 771
[31] Hayes W and Wilkens J 1964 *Proc. R. Soc.* A **281** 340
[32] Aramburu J A and Moreno M 1985 *J. Chem. Phys.* **83** 6071
[33] Aramburu J A, Moreno M and Barriuso M T 1987 *Cryst. Latt. Def. Amorph. Mater.* **16** 215
[34] Sugano S, Tanabe Y and Kamimura H 1970 *Multiplets of Transition-Metal Ions in Crystals* (New York: Academic)
[35] Messmer R P and Watkins G D 1973 *Phys. Rev.* B **7** 2568
[36] Basch H, Viste A and Gray H B 1966 *J. Chem. Phys.* **44** 10
[37] Ammeter J H, Burgi A B, Thibeault J C and Hoffmann R 1978 *J. Am. Chem. Soc.* **100** 3686
[38] Clementi E and Roetti C 1974 *At. Data Nucl. Data Tables* **14** 177
[39] Wang Y, Nordlander P and Tolk N H 1988 *J. Chem. Phys.* **89** 4163
[40] Kitamura M and Muramatsu S 1990 *Phys. Rev.* B **41** 1158
[41] Hong S Y and Marynick D S 1992 *J. Chem. Phys.* **96** 5497
[42] Johnson K H 1973 *Adv. Quantum Chem.* **7** 143
[43] Norman J G 1976 *Mol. Phys.* **31** 1191
[44] Aramburu J A and Moreno M 1987 *Solid State Commun.* **62** 513
[45] Wolfsberg M and Helmholz L 1952 *J. Chem. Phys.* **20** 837
[46] Aramburu J A, Moreno M and Bencini A 1987 *Chem. Phys. Lett.* **140** 462
[47] Breñosa G, Moreno M and Rodriguez F 1987 *Solid State Commun.* **63** 543
[48] Francisco E, Florez M, Barandiarán Z, Fernández Rodrigo G, Luaña V, Recio J M, Bermejo M, Seijo L and Pueyo L 1987 *Cryst. Latt. Def. Amorph. Mater.* **15** 45
[49] Moreno M 1989 *Cryst. Latt. Def. Amorph. Mater.* **18** 263
[50] Ohta Y, Tohyama T and Maekawa S 1991 *Phys. Rev. Lett.* **66** 1228

[51] Fernández Rodrigo G, Flórez M, Pueyo L, Moreno M and Barriuso M T 1987 *Cryst. Latt. Def. Amorph. Mater.* **16** 281
[52] Moreno M and Barriuso M T 1990 *Solid State Commun.* **75** 133
[53] Barriuso M T and Moreno M 1982 *Phys. Rev.* B **26** 2271
[54] Pauling L 1960 *The Nature of the Chemical Bond* (Ithaca, NY: Cornell University Press)
[55] Kan'no K, Naoe S, Mukai S and Nakai Y 1973 *Solid State Commun.* **13** 1325
[56] Kan'no K, Mukai S and Nakai Y 1974 *J. Phys. Soc. Japan* **36** 1492
[57] Hayashi M, Nakagawa H and Matsumoto H 1978 *Mem. Fac. Eng. Fukui Univ.* **26** 15
[58] Simonetti J and McClure D S 1979 *J. Chem. Phys.* **71** 793
[59] Hirako S and Onaka R 1982 *J. Phys. Soc. Japan* **51** 1255
[60] Borcherts R H, Kanzaki H and Abe H 1970 *Phys. Rev.* B **2** 23
[61] Chow C, Chang K and Willett R D 1973 *J. Chem. Phys.* **59** 2629
[62] Desjardins S R, Penfield R W, Cohen S L, Musselman R L and Solomon E I 1983 *J. Am. Chem. Soc.* **105** 4590
[63] McDonald R G and Hitchman M A 1986 *Inorg. Chem.* **25** 3273
[64] Cassidy P and Hitchman M A 1977 *Inorg. Chem.* **16** 1568
[65] Jørgensen C K 1970 *Prog. Inorg. Chem.* **12** 101
[66] Aramburu J A and Moreno M 1986 *Solid State Commun.* **58** 305
[67] Friebel C 1974 *Solid State Commun.* **15** 639
[68] Bill H, Lovy D and Hagemann H 1989 *Solid State Commun.* **7** 511
[69] Sierro J 1967 *J. Phys. Chem. Solids* **28** 417
[70] Yosida T, Aoki H, Takeuchi H, Arakawa M and Horai K 1991 *J. Phys. Soc. Japan* **60** 625
[71] Studzinski P, Casas-González J and Spaeth J M 1984 *J. Phys. C: Solid State Phys.* **17** 5411
[72] Agladze N I, Popova M N, Zhizhin G N, Egorov V J and Petrova M A 1991 *Phys. Rev. Lett.* **66** 447
[73] Di Bartolo B 1968 *Optical Interactions in Solids* (New York: Wiley)
[74] Monnier A, Gerber A and Bill H 1991 *J. Chem. Phys.* **94** 5891